HEPATOBILIARY-PANCREAS

Microvascular invasion of small hepatocellular carcinoma can be preoperatively predicted by the 3D quantification of MRI

San-Yuan Dong[1] · Wen-Tao Wang[1] · Xiao-Shan Chen[1] · Yu-Tao Yang[1] · Shuo Zhu[1] · Meng-Su Zeng[1] · Sheng-Xiang Rao[1]

Abstract

Objectives To explore the importance of three-dimensional (3D) quantitative analysis during gadoxetic acid–enhanced magnetic resonance imaging (MRI) of microvascular invasion (MVI) and early recurrence (< 2 years) after surgery of single hepatocellular carcinoma (HCC) ≤ 3 cm.

Methods Two hundred fourteen patients with pathologically confirmed HCC (training cohort: $n = 169$; validation cohort: $n = 45$) were included retrospectively. The 3D quantitative parameters (volume, sphericity, and compacity) and conventional MRI features were analyzed. The significant predictors for MVI were identified using univariate and multivariate logistic regression analyses. Nomograms were constructed from the prediction model, and the relationship between the significant predictors and early recurrence rates was evaluated using the Kaplan–Meier method.

Results Tumor sphericity (odds ratio [OR] = 0.000; $p < 0.001$), non-smooth tumor margin (OR = 3.353; $p = 0.015$), and peritumoral hypointensity on hepatobiliary phase (HBP) (OR = 14.067; $p = 0.003$) were independent significant factors for MVI. When these three factors were combined, the diagnostic specificity of the training and validation cohorts was 97.0 (128/132) and 87.9 (29/33), respectively. The nomogram based on the predictive model performed satisfactorily in the training (C-index: 0.885) and validation (C-index: 0.869) cohorts. Early recurrence rates of patients with two or three significant factors were significantly higher than those with none in the training (29.1% vs. 10.2%, $p = 0.007$) and validation (36.4% vs. 6.7%, $p = 0.037$) cohorts.

Conclusions Lower sphericity combined with non-smooth tumor margin and peritumoral hypointensity on HBP are potential predictive factors for MVI and associated with early recurrence after surgery of HCC ≤ 3 cm.

Key Points
- *Lower sphericity, non-smooth tumor margin, and peritumoral hypointensity on HBP were important indicators of the occurrence of MVI in HCC.*
- *The combinational model prepared from these findings satisfactorily predicted MVI, and the presence of these predictors was associated with an early recurrence rate after surgical resection in HCC patients.*
- *This model could help clinicians in the preoperative management of small HCC ≤ 3 cm.*

Abbreviations

3D	Three-dimensional
ADC	Apparent diffusion coefficient
AFP	Alpha-fetoprotein
AUC	Area under the curve
CI	Confidence interval
CT	Computed tomography
DWI	Diffusion-weighted imaging
HBP	Hepatobiliary phase
HCC	Hepatocellular carcinoma
ICC	Intraclass correlation coefficients
MRI	Magnetic resonance imaging
MVI	Microvascular invasion
NPV	Negative predictive value
OATP	Organic anion-transporting polypeptide
OR	Odds ratio
PACS	Picture archiving and communication system
PPV	Positive predictive value

✉ Sheng-Xiang Rao
raoxray@163.com

1 Department of Radiology, Institute of Medical Imaging, Zhongshan Hospital, Fudan University, Xuhui District, No. 180 Fenglin Road, Shanghai 200032, China

RFA   Radiofrequency ablation
ROC   Receiver operating characteristic
ROI   Regions of interest
SI   Signal intensity
VIBE   Volumetric-interpolated breath-hold examination

Introduction

Hepatocellular carcinoma (HCC) is one of the most widespread neoplasms and is the third global cause of cancer-related deaths [1]. Microvascular invasion (MVI) is a significant risk factor responsible for tumor recurrence, specifically early recurrence, in HCC patients [2, 3]. The incidence of MVI in small HCC ≤ 3 cm is 18.1 to 37.0% [4, 5]. For patients with MVI-positive small HCC, surgical resection proves more beneficial than radiofrequency ablation (RFA) because the former technique is capable of clearing a larger percentage of micrometastasis. Furthermore, anatomic resection (complete removal of tumor-bearing portal territory) can avert early recurrence [2, 3, 6]. However, the major drawback lies in the fact that MVI is detected by histological examination after surgery. Therefore, it is important to explore methods that identify MVI at the preoperative stage.

Gadoxetic acid–enhanced magnetic resonance imaging (MRI) is highly sensitive in detecting HCC [7, 8]. Literature reports indicate the capability of specific MRI features in predicting the presence of MVI in HCC [9–11]. However, these features have limited capacities. Radiomics and deep learning are emerging methods utilized for predicting MVI in HCC. However, they are burdened by several key problems, such as the stability of high-throughput data, modeling methodology, and evaluation criteria [12–14].

The macroscopic classification of HCC is associated with MVI. The recurrence of the single nodular type with extra-nodular growth, confluent multinodular type, and infiltrative type is higher than that of the single nodular type [15, 16]. High-resolution images obtained from gadoxetic acid–enhanced MR can classify HCC at the macroscopic level. However, the interobserver agreement among the reviewers is not strong [17, 18]. Three-dimensional (3D) quantitative analysis is a technique that furnishes a more detailed and repeatable quantitative assessment of the tumor characteristics. Reports indicate the application of 3D quantitative parameters extracted from tumor lesions in preoperative diagnosis and risk stratification. Additionally, they display strong interobserver agreement [19–21]. These results enabled the hypothesis that 3D quantitative analysis of gadoxetic acid–enhanced MRI may help predict MVI in HCC.

Thus, the current study aimed to explore the significance of preoperative 3D quantitative analysis and imaging features of gadoxetic acid–enhanced MR in MVI and the relationship between the significant predictors and early recurrence after surgery of single HCC ≤ 3 cm.

Material and methods

The institutional review board approved this retrospective study, and informed consent from the participants was waived.

Study design

The patients were divided into the training cohort and the validation cohort according to time. The data from the training cohort enabled the screening of the significant image features and established the MVI prediction model. The data from the validation cohort verified the diagnostic performance of the prediction model.

Patients

Consecutive patients who underwent gadoxetic acid–enhanced MRI before HCC surgical resection between March 2012 and October 2019 were retrospectively included. The patients with the following criteria were as included: pathologically proven single HCC without suspicious lymph nodes, longest tumor diameter ≤ 3 cm in MR imaging, and examination of gadoxetic acid–enhanced MRI within 30 days before surgery. The inclusion and exclusion criteria are summarized in the patient flow diagram shown in Fig. 1.
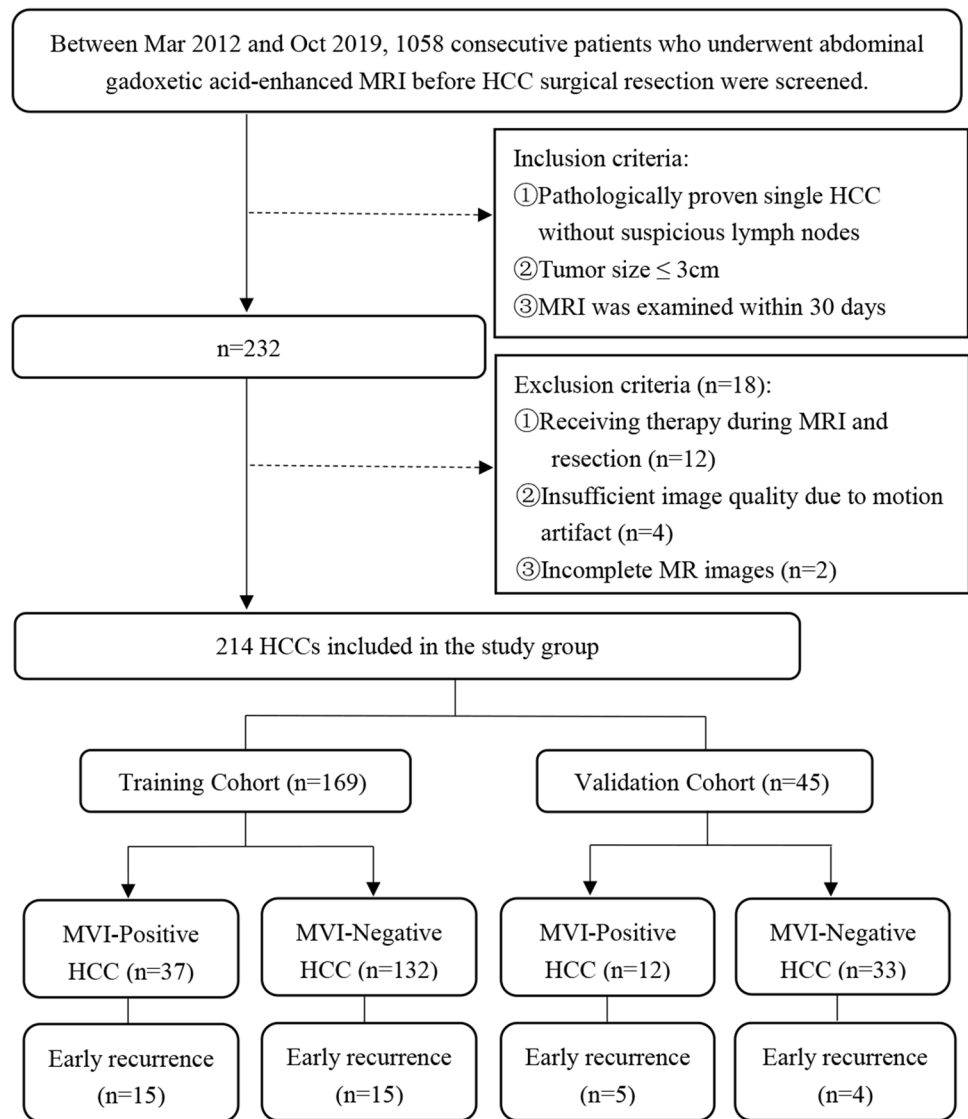
MR imaging data

All patients were scanned in a 1.5 T scanner (MAGNETOM Aera, Siemens Healthcare) and administered an intravenous bolus injection of 0.025 mmol/kg gadoxetic acid (Primovist, Bayer HealthCare Pharmaceuticals Inc.). The following MRI sequences were recorded: diffusion-weighted imaging (DWI), T2-weighted phase with fat suppression, pre-contrast T1-weighted phase and post-contrast dynamic T1-weighted volumetric-interpolated breath-hold examination (VIBE) at arterial phase (20–30 s), portal venous phase (60–70 s), transitional phase (180 s), and hepatobiliary phase (HBP, 20 min). The details of these MRI sequences are summarized in Table S1.

Imaging analysis

The image features analyzed in this study included 3D quantification parameters, traditional quantitative image features, and qualitative image features. Three radiologists (with 6, 8, and 18 years of experience in abdominal image diagnosis,

Fig. 1 Flow diagram showing the inclusion and exclusion criteria for the study

Between Mar 2012 and Oct 2019, 1058 consecutive patients who underwent abdominal gadoxetic acid-enhanced MRI before HCC surgical resection were screened.

Inclusion criteria:
①Pathologically proven single HCC without suspicious lymph nodes
②Tumor size ≤ 3cm
③MRI was examined within 30 days

n=232

Exclusion criteria (n=18):
①Receiving therapy during MRI and resection (n=12)
②Insufficient image quality due to motion artifact (n=4)
③Incomplete MR images (n=2)

214 HCCs included in the study group

Training Cohort (n=169)

Validation Cohort (n=45)

MVI-Positive HCC (n=37)

MVI-Negative HCC (n=132)

MVI-Positive HCC (n=12)

MVI-Negative HCC (n=33)

Early recurrence (n=15)

Early recurrence (n=15)

Early recurrence (n=5)

Early recurrence (n=4)

respectively; hereafter referred to as reader 1, reader 2, and reader 3, respectively) participated in the lesion image evaluation. Reader 1 and reader 3 evaluated the quantitative image features, and reader 2 and reader 3 together investigated the qualitative image features.

3D quantitative analysis

The entire tumor segmentation exercise was accomplished using the LIFEx software (http://www.lifexsoft.org). Earlier reports have indicated that the boundary of the lesion is best visualized on the HBP images [22, 23]. Hence, in the current study, the regions of interest (ROI) were manually drawn along the tumor boundary on the HBP images. The tumors were first segmented by reader 1. Next, tumor segmentation was independently performed by reader 3 on randomly chosen 50 lesions (40 in the training cohort and 10 in the

validation cohort) to test the reproducibility of the features extracted from the segmentation [24]. Both reviewers were aware of the HCC diagnosis but blinded to clinical, laboratory, histopathological, and follow-up results. The HCC contouring on MR images is shown in Fig. 2.

After profiling the entire tumor, three 3D quantitative parameters were calculated using the LIFEx software: (1) volume (mL), the volume of interest in mL; (2) sphericity, ranging from 0 to 1. The sphericity of a perfect sphere is equal to 1; (3) compacity, reflecting how compact the lesion is. The 3D shape parameter formulae are given in the supplementary material.

Traditional imaging features

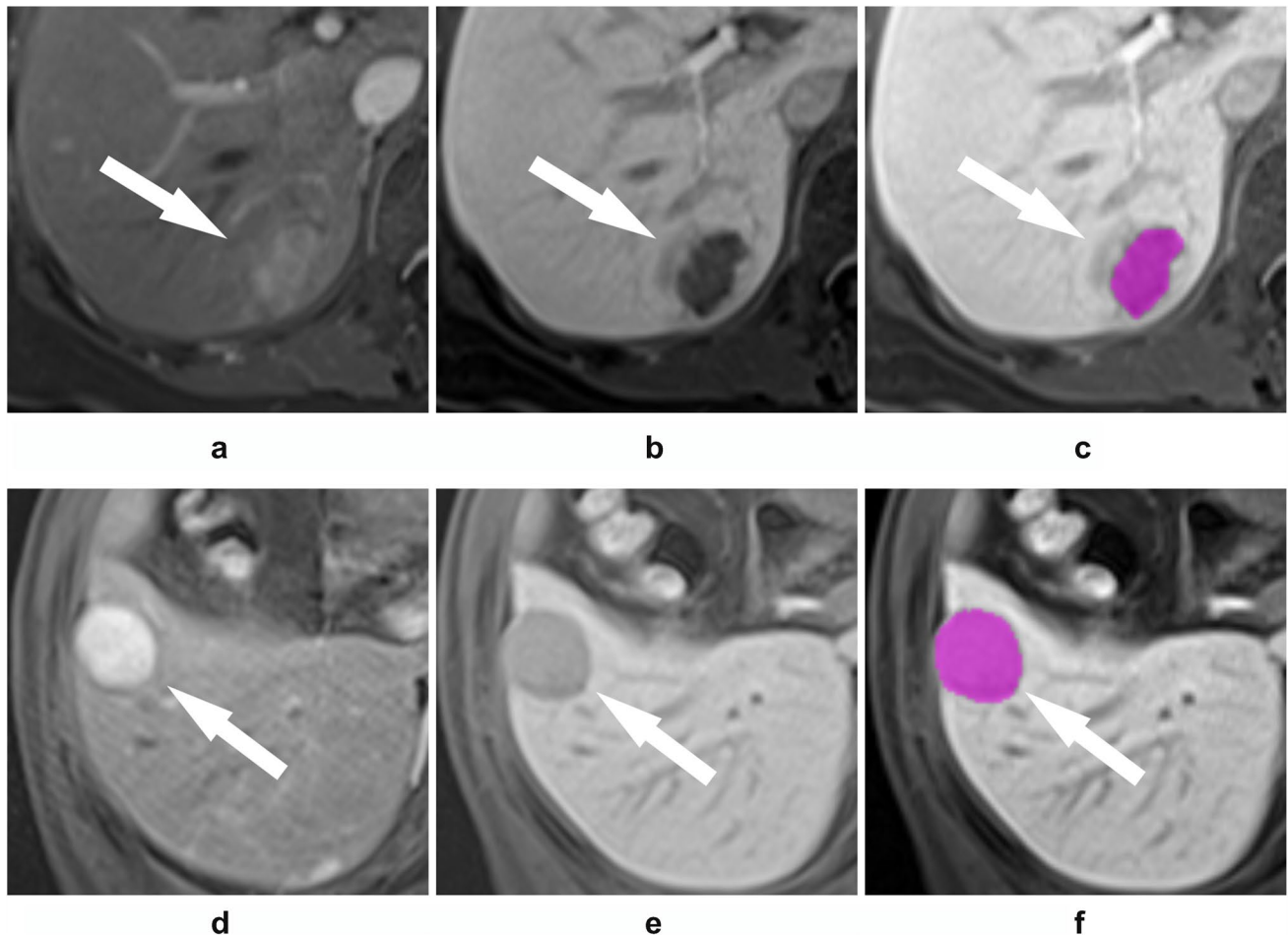The following traditional quantitative image features were recorded: tumor size, tumor apparent diffusion coefficient

Fig. 2 Examples of small HCC. **a–c** Hepatocellular carcinoma with microvascular invasion in a 61-year-old woman. Tumor recurrence occurred in the liver 8 months after surgical resection. **a** Gadoxetic acid–enhanced arterial phase MR image shows a 2.8-cm hypervascular mass with peritumoral enhancement in the hepatic segment VI. **b** Hepatobiliary phase image shows as non-smooth tumor margin and peritumoral hypointensity. **c** Segmentation display at this level of the lesion on the HBP images. The tumor sphericity is 0.730. **d–f** Hepatocellular carcinoma without microvascular invasion in a 49-year-old man. Tumor recurrence did not occur during 24 months of the follow-up period after surgical resection. **d** Gadoxetic acid–enhanced arterial phase MR image shows a 2.9-cm hypervascular mass without peritumoral enhancement in the hepatic segment V. **e** Hepatobiliary phase image shows smooth tumor margin and no peritumoral hypointensity. **f** Segmentation display at this level of the lesion on the HBP images. The tumor sphericity is 0.818

(ADC) value, tumor-to-liver signal intensity (SI) ratio on DWI, and tumor-to-liver SI ratio on HBP. The maximum diameter on the transverse images defined the tumor size. The other parameters were measured at the level of the maximum diameter of the tumor. Manually, the ROI was placed on the ADC map, DWI (b value of 500 s/mm^2), and HBP images to approximately include the entire tumor area. The peripheral portions were excluded to prevent interference by partial volume effects from the adjacent tissue. All lesions were first measured by reader 1. Reader 3 then independently measured 50 randomly chosen lesions (same as those mentioned in "3D quantitative analysis") to evaluate interobserver reproducibility. Further details are given in the supplementary material.

The qualitative image features were independently reviewed by reader 2 and reader 3 by a picture archiving and communication system (PACS). The two readers arrived at a consensus, and a final decision was made regarding the inconsistent cases. The following qualitative imaging features were evaluated: (a) arterial rim enhancement, (b) arterial peritumoral enhancement, (c) tumor margin, (d) tumor capsule, (e) tumor hypointensity on HBP, (f) peritumoral hypointensity on HBP, and (g) enhancement pattern. The qualitative imaging features are described in the supplementary material.

Histopathological diagnosis and follow-up

The appearance of tumor emboli in the tiny blood vessels in the vicinity of the primary tumor is defined as MVI; the emboli can be visualized only microscopically. The histopathological data were obtained from surgical and pathologic reports completed initially by two experienced pathologists (with 15 and 21 years of experience in liver histopathological diagnosis, respectively). The etiology of liver disease for the patients recruited in the current study included chronic viral hepatitis B, viral hepatitis C, and others (alcohol intake and aflatoxin exposure). The number of cases with the respective etiologies is given in Table 1. After surgical resection, the patients were monitored with multiphase liver computed tomography (CT) or MRI and alpha-fetoprotein (AFP) every 3–6 months to evaluate tumor recurrence. Early recurrence was defined as an occurrence within 2 years after surgery of HCC [25].

Nomogram construction and evaluation

The nomogram was constructed from the predictive model and illustrated graphically. Harrell's C-index evaluated the discrimination performance of the nomogram. Calibration curves analyzed the diagnostic performance of the nomogram in the training and validation cohorts. The decision curve determined the clinical efficacy of the nomogram by quantifying the net benefits of the entire cohort under different threshold probabilities.

Table 1 Patient characteristics

Variable	Training cohort (n = 169)			Validation cohort (n = 45)			p value
	MVI (+)	MVI (-)	p value	MVI (+)	MVI (-)	p value	0.498
Age (years)[*]	57.2 ± 10.0	53.7 ± 11.5	0.100	57.5 ± 10.6	54.6 ± 10.4	0.408	0.643
Gender			0.513			0.419	0.414
Male	31 (83.8)	116 (87.9)		11 (91.7)	26 (78.8)		
Female	6 (16.2)	16 (12.1)		1 (8.3)	7 (21.2)		
Intrahepatic location			0.578			0.691	0.416
Right	31 (83.8)	101 (76.5)		8 (66.7)	23 (70.0)		
Left	5 (13.5)	28 (21.2)		4 (33.3)	9 (27.3)		
Caudate lobe or border area	1 (2.7)	3 (2.3)		0 (0)	1 (2.7)		
Background liver tissue			0.520			0.746	0.475
Liver cirrhosis	27 (73.0)	89 (67.4)		7 (58.3)	21 (63.6)		
None	10 (27.0)	43 (32.6)		5 (41.7)	12 (36.4)		
Etiology of liver disease			0.723			0.467	0.487
Hepatitis B virus	35 (94.6)	123 (93.2)		11 (91.7)	32 (97.0)		
Hepatitis C virus	1 (2.7)	2 (1.5)		0 (0)	0 (0)		
None or other	1 (2.7)	7 (5.3)		1 (8.3)	1 (3.0)		
Edmondson-Steiner grade			0.003			0.222	0.721
G1-G2	15 (40.5)	89 (67.4)		6 (50.0)	23 (70.0)		
G3-G4	22 (59.5)	43 (32.6)		6 (50.0)	10 (30.0)		
Satellite nodule			0.510			0.561	1.000
Presence	4 (10.8)	10 (7.6)		0 (0)	4 (12.1)		
Absence	33 (89.2)	122 (92.4)		12 (100.0)	29 (87.9)		
Serum AFP			0.723			0.648	0.572
< 20 ng/mL	19 (51.4)	77 (58.3)		8 (66.6)	21 (63.6)		
20–400 ng/mL	14 (37.8)	41 (31.1)		2 (16.7)	9 (27.3)		
> 400 ng/mL	4 (10.8)	14 (10.6)		2 (16.7)	3 (9.1)		
Total bilirubin			0.369			0.721	0.001
≤ 20.4 μmol/L	35 (94.6)	117 (88.6)		8 (66.7)	24 (72.7)		
> 20.4 μmol/L	2 (5.4)	15 (11.4)		4 (33.3)	9 (27.3)		

Unless otherwise indicated, data are the number of patients, with the percentage in parentheses. AFP, alpha-fetoprotein; MVI, microvascular invasion

[*]Data are continuous variables, reported as means ± standard deviations

Statistical analysis

The statistical differences among the variables were evaluated using the two-sample *t*-test or the Mann–Whitney *U* test for continuous variables and the chi-square test or Fisher's exact test for categorical variables. Univariate and multivariate logistic regression analyses assessed the independent risk factors for MVI. Nomograms were built using this prediction model. Statistically significant variables were further investigated using the receiver operating characteristic (ROC) curve analysis. The model's capacity to predict MVI was calculated from the area under the curve (AUC). The best cutoff values for ROC curves were determined using Youden's index. Interobserver agreement on qualitative and quantitative image findings was determined using kappa statistics and intraclass correlation coefficients (ICC), respectively. These values are explained as follows: 0.00–0.20, no agreement; 0.21–0.40, weak agreement; 0.41–0.60, moderate agreement; 0.61–0.80, strong agreement; and 0.81–1.0, almost perfect agreement. The sensitivity, specificity, accuracy, positive predictive value (PPV), and negative predictive value (NPV) of each significant imaging finding and the combinations of the findings that predicted MVI were also calculated. Early recurrence curves were evaluated by using the Kaplan–Meier method, and differences among the subgroups were compared by the log-rank test. All statistical analyses were performed on the SPSS software (version 26.0) and R software (version 3.6.1). $p < 0.05$ indicated statistical significance.

Results

Demographic and pathologic characteristics

Table 1 shows the baseline clinical and pathologic characteristics of HCC. The final cohort of 214 patients (184 men and 30 women) was classified into two cohorts. The training cohort included 169 patients (37 for MVI-positive, 132 for MVI-negative; 147 men and 22 women) and was conducted from March 2012 to December 2017. The time-independent validation cohort involved 45 patients (12 for MVI-positive, 33 for MVI-negative; 37 men and 8 women) and was conducted from January 2018 to October 2019.

In the training cohort, statistical difference between the MVI-positive and MVI-negative groups was observed only in the Edmondson-Steiner grade ($p = 0.003$). However, this was a postoperative feature and not included in the multivariate analysis. Other baseline variables, including age, gender, background liver, and etiology of liver disease, were similar in both groups ($p > 0.05$). No significant difference was observed between the training cohort and the validation cohort considering other variables; total bilirubin ($p = 0.001$)

was an exception. No significant difference was observed in the MVI status between the two cohorts ($p = 0.498$).

MR imaging characteristics

The quantitative MR imaging features of HCC are described in Table 2. In the training cohort, statistical differences between the MVI-positive and MVI-negative patients were observed in the following image features: tumor volume ($p < 0.001$), sphericity ($p < 0.001$), compacity ($p = 0.002$), tumor size ($p < 0.001$), and tumor-to-liver SI ratio on DWI ($p = 0.034$). The ICCs for the imaging findings were 0.913–0.980 ($p < 0.001$). The tumor volume of HCCs with MVI was larger than that of HCCs lacking MVI. The tumor sphericity of HCCs with MVI was smaller than that of HCCs without MVI, suggesting that the MVI-positive HCC lesions were less spherical. The tumor compacity of the HCCs with MVI was larger than that of HCCs without MVI, suggesting the more compact nature of the MVI-positive HCC lesions. The tumor size and tumor-to-liver SI ratio on DWI of the HCCs with MVI were larger than the respective parameters of the HCCs without MVI. No statistical difference was identified in the quantitative imaging features between the training and the validation cohorts ($p > 0.05$).

The qualitative MR imaging findings of HCC are described in Table 3. In the training cohort, statistical difference between the MVI-positive and MVI-negative patients was observed in the following image features: arterial peritumoral enhancement ($p = 0.001$), non-smooth tumor margin ($p < 0.001$), and peritumoral hypointensity on HBP ($p < 0.001$). Cohen's kappa coefficients for the imaging results were 0.774–0.841 ($p < 0.001$). No statistical difference was identified in the qualitative imaging features between the training and the validation cohorts ($p > 0.05$).

Prediction model

The results of the univariate and multivariate analyses of imaging findings related to MVI expression in the training cohort are described in Table 4. The variables showing $p < 0.05$ in the univariate logistic regression analysis were applied to multivariate logistic regression analysis. Statistical difference was observed in the tumor sphericity (odds ratio [OR], 0.000; $p < 0.001$), non-smooth tumor margin (OR, 3.353; $p = 0.015$), and peritumoral hypointensity on HBP (OR, 14.067; $p = 0.003$) finally for MVI in HCC. The optimal tumor sphericity cutoff value of 0.800 was obtained based on Youden's index of the ROC.

The sensitivity, specificity, accuracy, PPV, and NPV for predicting MVI using the three significant factors and their combinations are described in Table 5. In the training cohort, the combination of all three factors produced the values of 45.9 (17/37) for sensitivity, 97.0 (128/132) for

Table 2 Quantitative MR imaging findings

Variable	Training cohort (n = 169)				Validation cohort (n = 45)				p value
	MVI (+)	MVI (-)	p value	ICC	MVI (+)	MVI (-)	p value	ICC	0.498
Volume (mL)	3.946 (1.335, 5.640)	1.254 (0.596, 3.441)	<0.001	0.980	3.164 (0.844, 8.165)	2.094 (1.358, 7.090)	0.080	0.990	0.109
Sphericity	0.765 (0.731, 0.798)	0.813 (0.793, 0.834)	<0.001	0.950	0.746 (0.717, 0.795)	0.807 (0.775, 0.824)	0.003	0.973	0.122
Compacity	2.494 (1.762, 2.769)	1.798 (1.437, 2.540)	0.002	0.953	2.221 (1.867, 3.009)	1.938 (1.478, 3.067)	0.488	0.916	0.121
ADC value	1.174 (0.989, 1.457)	1.224 (0.996, 1.461)	0.741	0.926	1.038 (0.814, 1.281)	1.182 (1.003, 1.368)	0.293	0.947	0.281
Tumor size (cm)	2.000 (1.450, 2.500)	1.500 (1.000, 1.900)	<0.001	0.913	2.350 (1.500, 2.725)	2.000 (1.100, 2.600)	0.469	0.951	0.117
Tumor-to-liver SI ratio on DWI	1.750 (1.473, 2.273)	1.637 (1.349, 1.959)	0.034	0.971	1.723 (1.324, 1.878)	1.577 (1.253, 1.821)	0.441	0.978	0.253
Tumor-to-liver SI ratio on HBP	0.574 (0.495, 0.659)	0.594 (0.522, 0.710)	0.140	0.942	0.488 (0.438, 0.628)	0.610 (0.490, 0.707)	0.137	0.896	0.254

Data are median (interquartile range). *ADC* apparent diffusion coefficient; *SI* signal intensity; *DWI* diffusion-weighted imaging; *HBP* hepatobiliary phase; *MVI* microvascular invasion; *ICC* intraclass correlation coefficients

Table 3 Qualitative MR imaging findings

Variable	Training cohort (n = 169)				Validation cohort (n = 45)				p value
	MVI (+)	MVI (-)	p	Kappa	MVI (+)	MVI (-)	p	Kappa	0.498
Arterial rim enhancement			0.424	0.868			1.000	0.775	0.527
Presence	7 (18.9)	18 (13.6)			1 (8.3)	4 (12.1)			
Absence	30 (81.1)	114 (86.4)			11 (91.7)	29 (87.9)			
Arterial peritumoral enhancement			0.001	0.835			0.499	0.818	0.630
Presence	22 (59.5)	39 (29.5)			6 (50.0)	12 (36.4)			
Absence	15 (40.5)	93 (70.5)			6 (50.0)	21 (63.6)			
Tumor margin			<0.001	0.774			0.001	0.815	0.594
Non-smooth	27 (73.0)	37 (28.0)			10 (83.3)	9 (27.3)			
Smooth	10 (27.0)	95 (72.0)			2 (16.7)	24 (72.7)			
Tumor capsule			0.393	0.775			0.076	0.793	0.324
Complete	27 (73.0)	105 (79.5)			6 (50.0)	26 (78.8)			
Incomplete or absent	10 (27.0)	27 (20.5)			6 (50.0)	7 (21.2)			
Tumor hypointensity on HBP			1.000	0.854			1.000	1.000	1.000
Presence	37 (100.0)	129 (97.7)			12 (100.0)	32 (97.0)			
Absence	0 (0)	3 (2.3)			0 (0)	1 (3.0)			
Peritumoral hypointensity on HBP			<0.001	0.841			0.017	0.822	0.147
Presence	24 (64.9)	28 (21.2)			10 (100.0)	13 (39.4)			
Absence	13 (35.1)	104 (78.8)			2 (0)	20 (60.6)			
Enhancement pattern			0.445	0.769			0.162	0.915	0.227
Arterial enhancement with washout	28 (75.7)	108 (81.8)			8 (66.7)	20 (60.6)			
No or minimal enhancement	4 (10.8)	8 (6.1)			4 (33.3)	12 (36.4)			
Persistent enhancement	3 (8.1)	14 (10.6)			0 (0)	1 (3.0)			
Progressive enhancement	2 (5.4)	2 (1.5)			0 (0)	0 (0)			

Data are the number of patients, with the percentage in parentheses. *HBP* hepatobiliary phase; *MVI* microvascular invasion

Table 4 Univariate and multivariate analyses for predicting MVI-positive HCC in the training cohort

Variable	Univariate analysis		Multivariate analysis	
	Odds ratio (95% CI)	p value	Odds ratio (95% CI)	p value
Tumor size (mm)	3.210 (1.754–5.876)	< 0.001	1.377 (0.346–5.479)	0.650
Tumor-to-liver SI ratio on DWI	1.747 (0.954–3.198)	0.071		
Volume (mL)	1.181 (1.045–1.334)	0.007	0.582 (0.292–1.162)	0.125
Sphericity	0.000 (0.000–0.000)	< 0.001	0.000 (0.000–0.000)	**< 0.001**[*]
Compacity	2.035 (1.202–3.447)	0.008	10.471 (0.556–19.092)	0.117
Non-smooth tumor margin	6.932 (3.056–15.724)	< 0.001	3.353 (1.263–8.905)	**0.015**[*]
Arterial peritumoral enhancement	3.497 (1.643–7.444)	0.001	0.274 (0.047–1.601)	0.151
Peritumoral hypointensity on HBP	6.857 (3.101–15.162)	< 0.001	14.067 (2.411–82.084)	**0.003**[*]

[*]Tumor sphericity, non-smooth tumor margin, and peritumoral hypointensity on HBP were independent significantfactors in multivariate analyses

SI signal intensity; *DWI* diffusion-weighted imaging; *HBP* hepatobiliary phase; *CI* confidence interval; *MVI* microvascular invasion; *HCC* hepatocellular carcinoma

Table 5 Diagnostic performance of significant imaging findings and combinations for predicting MVI-positive HCC

Variable (training cohort)	Sensitivity	Specificity	Accuracy	PPV	NPV
Sphericity < 0.800	78.4 (29/37)	68.9 (91/132)	71.0 (120/169)	41.4 (29/70)	91.0 (91/100)
Non-smooth tumor margin	73.0 (27/37)	72.0 (95/132)	72.2 (122/169)	42.2 (27/64)	90.5 (95/105)
Peritumoral hypointensity on HBP	64.9 (24/37)	79.5 (105/132)	76.3 (129/169)	47.1 (24/51)	89.0 (105/118)
Combination of any two findings	73.0 (27/37)	78.8 (104/132)	77.5 (131/169)	49.1 (27/55)	91.2 (104/114)
Combination of all three findings	45.9 (17/37)	97.0 (128/132)	85.8 (145/169)	81.0 (17/21)	86.5 (128/148)
Variable (validation cohort)					
Sphericity < 0.800	83.3 (10/12)	63.6 (21/33)	68.9 (31/45)	45.5 (10/22)	91.3 (21/23)
Non-smooth tumor margin	75.0 (9/12)	72.7 (24/33)	75.6 (34/45)	52.6 (10/19)	92.3 (24/26)
Peritumoral hypointensity on HBP	75.0 (9/12)	60.6 (20/33)	66.7 (30/45)	43.5 (10/23)	90.9 (20/22)
Combination of any two findings	83.3 (10/12)	63.6 (21/33)	68.9 (31/45)	45.5 (10/22)	91.3 (21/23)
Combination of all three findings	66.7 (8/12)	87.9 (29/33)	82.2 (37/45)	66.7 (8/12)	87.9 (29/33)

Data are presented as percentages. Data in parentheses are the number of subjects used to calculate the percentage. *HBP* hepatobiliary phase; *PPV* positive predictive value; *NPV* negative predictive value; *MVI* microvascular invasion; *HCC* hepatocellular carcinoma

specificity, and 85.8 (145/169) for accuracy. In the validation cohort, when all three factors were combined, the values for sensitivity, specificity, and accuracy were 66.7 (8/12), 87.9 (29/33), and 82.2 (37/45), respectively.

For the two cohorts, the diagnostic model was combined with the three significant factors. The resulting AUC values were 0.885 (95% confidence interval [CI]: 0.825, 0.946; training cohort) and 0.869 (95% CI: 0.753, 0.985; validation cohort) (Fig. 3). The diagnostic model (with the significant factors combined) exhibited the highest predictive value compared to that obtained using each significant MRI finding alone.

### Development and validation of the nomogram

The nomogram for predicting MVI using the three significant MR imaging findings is illustrated in Fig. 4. The training cohort (C-index 0.885) and the validation cohort (C-index 0.869) were predicted satisfactorily. The calibration

curves for prediction and observation agreed well in both cohorts. The net benefit of the decision curve for the predictive nomogram in the whole cohort was higher than that when it was assumed that all or no patients expressed MVI. Moreover, the threshold probability was between 1 and 85%, indicating that the therapy strategy based on our nomogram would be capable of improving clinical outcomes.

Early recurrence rates of patients

The early recurrence rates of patients with no, one, and two or three significant MR imaging findings are described in Fig. 5. In the training cohort, during the entire follow-up period (range, 28–731 days; median, 648 days), the recurrence rates of the three groups were 10.2% (6/59, no MR finding), 14.5% (8/55, one MR finding), and 29.1% (16/55, two or three MR findings), respectively. In the validation cohort, during the entire follow-up period (range,

Fig. 3 Receiver operating characteristic (ROC) curve of the three significant MR imaging findings and diagnostic model in the prediction of microvascular invasion for small hepatocellular carcinoma. **a** ROC curve in the training cohort; **b** ROC curve in the validation cohort. AUC: area under the curve
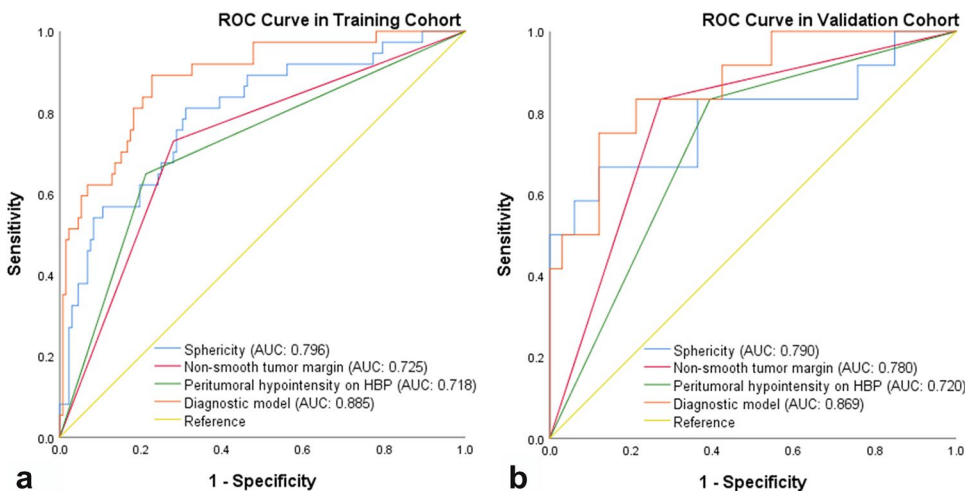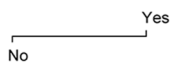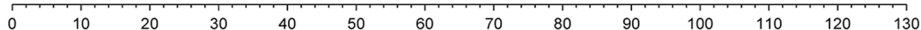

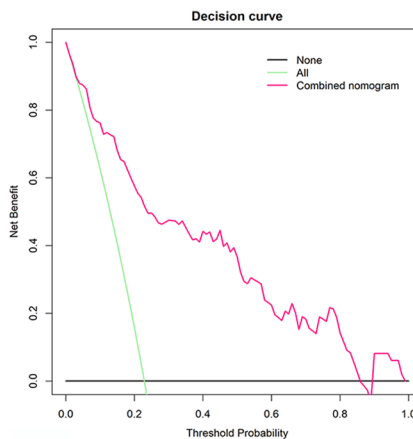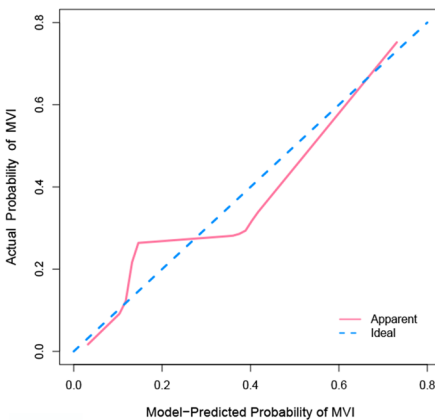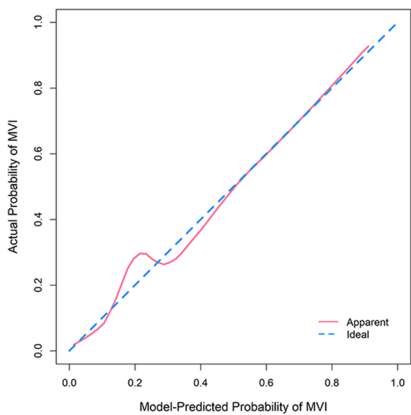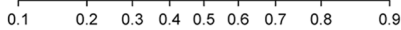**Fig. 4** Nomogram for preoperative estimation of microvascular invasion (MVI) risk and its predictive performance. **a** Nomogram for predicting MVI probabilities. When using the nomogram, find the position of each variable on the axis and the corresponding point was identified vertically. Then, the points of all variables were added and converted into the MVI-positive probability on the bottom scale. **b**, **c** Calibration curves of the nomogram in the training and validation cohorts. The X-axis is the nomogram-predicted probability of MVI; Y-axis is the observed MVI, and the diagonal dashed line represents the ideal prediction by a perfect model. **d** Decision curves of the nomogram in the whole cohort. The green line is the net benefit obtained by assuming that all patients have manifested MVI; the black line is the net benefit obtained by assuming that no patients have manifested MVI; the red line is the expected net benefit of per patient based on the predictive nomogram

Fig. 5 Early recurrence rates of patients. **a** In the training cohort. **b** In the validation cohort. Early recurrence rates of patients with single hepatocellular carcinoma with no (blue line), one (red line), and two or three (green line) significant MR imaging findings for predicting MVI
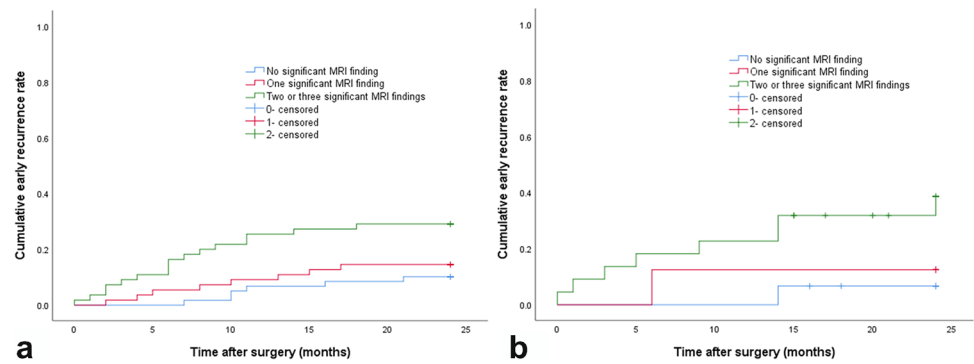
24–731 days; median, 701 days), the recurrence rates of the three groups were 6.7% (1/15), 12.5% (1/8), and 36.4% (8/22), respectively. Early recurrence rates of patients expressing two or three significant factors were significantly higher than the patients that manifested no significant factors in the training (29.1% vs. 10.2%, $p = 0.007$) and the validation cohorts (36.4% vs. 6.7%, $p = 0.037$).

Discussion

In the present study, tumor sphericity, non-smooth tumor margin, and peritumoral hypointensity on gadoxetic acid–enhanced HBP were identified as independent and significant variables that predicted MVI in single HCC ≤ 3 cm. Moreover, these factors exhibited good interobserver agreement. The diagnostic specificity and accuracy of MVI were higher when the three MRI findings were combined. The nomogram constructed from the prediction model was predicted satisfactorily and calibrated well in both cohorts. Additionally, the early recurrence rate in patients with two or three MR imaging findings was significantly higher than that in patients without any MRI findings after surgery in both cohorts.

Tumor sphericity manifested as a significant MRI finding for predicting MVI in 3D quantitative analysis in the current study. This observation is consistent with previous results that described the significance of tumor sphericity in tumor preoperative diagnosis and risk stratification [19–21]. The macroscopic appearance of single nodular type with extranodular growth, confluent multinodular type, and infiltrative type indicates low tumor sphericity. The single nodular type corresponds to high tumor sphericity because tumors with longer shapes or more protrusions presented lower sphericity. Moreover, literature reports have indicated a higher postoperative recurrence rate of the single nodular type with extra-nodular growth, confluent multinodular type, and infiltrative type of HCCs than that of the single nodular type HCCs [15, 16].

Non-smooth tumor margin was an important MRI finding for predicting MVI in the present study, and this

observation was consistent with that from previous studies [9, 26]. The aggressive biological tendencies of HCC for invading the tumor capsule and protrusion into the non-tumoral parenchyma are demonstrated by non-smooth tumor margins. Previous studies have related non-smooth tumor margin with early recurrence of HCC [26, 27].

Peritumoral hypointensity on HBP images was another important factor that predicted MVI in the current study. This observation was also consistent with those from previous studies [26, 28]. Peritumoral perfusion changes caused by MVI affect the organic anion-transporting polypeptide (OATP) expression of the hepatocyte membrane around the tumor. This changes the hepatic function and reduces the uptake of gadoxetic acid by hepatocytes around the tumors. This could be the probable mechanism of peritumoral hypointensity on HBP images of HCC with MVI. Additionally, previous studies have shown that the peritumoral hypointensity on HBP was related to the early recurrence of HCC [29, 30].

Total bilirubin was significantly different between the training cohort and the validation cohort, possibly due to the selection bias of the retrospective nature of the study. However, there was no significant difference in the other clinical-pathological variables, MVI states, and imaging features between the two cohorts. Thus, the data were similar between the training and the validation cohorts in the present study.

The current study exhibited good diagnostic performance in predicting MVI in HCC. When the three significant imaging findings of tumor sphericity ($p < 0.800$), non-smooth tumor margin, and peritumoral hypointensity on HBP were combined, the diagnostic specificity and accuracy of MVI increased in the two cohorts. The nomogram based on the prediction model performed satisfactorily in the two cohorts and with good calibration. The predictive nomograms based on clinical-radiological factors of previous studies [31, 32] were not as accurate as those obtained in the current study. Therefore, the current nomogram was capable of improving the diagnostic performance of MVI prediction. This nomogram might assist surgeons in treatment decision-making and promote a personalized therapeutic regime for HCC patients.

The current study confirmed that patients manifesting two or three significant MRI findings had a significantly higher early recurrence rate than patients with none of the findings after HCC radical resection in both cohorts. The combination of significant MR imaging findings for predicting MVI might have a synergistic effect in predicting early recurrence of HCC preoperatively, compared to each significant MRI finding considered individually.

The study has several limitations. First, the retrospective study design could result in selection bias. Second, the tumor size was limited to less than 3 cm in the study. Hence, the results cannot be generalized to HCCs that contain tumors with the largest diameter greater than 3 cm. Third, only the quantitative 3D parameters on HBP were analyzed; the differences among the sequences were not compared. Finally, the pathological macroscopic classification of HCC was not compared with the quantitative characteristics of HCC.

In conclusion, lower sphericity in 3D quantitative analysis, non-smooth tumor margin, and peritumoral hypointensity on HBP can function as preoperative imaging biomarkers for speculating MVI with good predictive performance. These factors are associated with early recurrence after surgery of single HCC ≤ 3 cm.

Declarations

References

1. Siegel RL, Miller KD, Fuchs HE, Jemal A (2021) Cancer statistics, 2021. CA Cancer J Clin 71:7–33
2. Lee S, Kang TW, Song KD et al (2021) Effect of microvascular invasion risk on early recurrence of hepatocellular carcinoma after surgery and radiofrequency ablation. Ann Surg 273:564–571
3. Erstad DJ, Tanabe KK (2019) Prognostic and therapeutic implications of microvascular invasion in hepatocellular carcinoma. Ann Surg Oncol 26:1474–1493
4. Giuliante F, Ardito F, Pinna AD et al (2012) Liver resection for hepatocellular carcinoma ≤3 cm: results of an Italian multicenter study on 588 patients. J Am Coll Surg 215:244–254
5. Du M, Chen L, Zhao J et al (2014) Microvascular invasion (MVI) is a poorer prognostic predictor for small hepatocellular carcinoma. BMC Cancer 14:38
6. Zhang EL, Cheng Q, Huang ZY, Dong W (2021) Revisiting surgical strategies for hepatocellular carcinoma with microvascular invasion. Front Oncol 11:691354
7. European Association for the Study of the Liver (2018) EASL Clinical Practice Guidelines: management of hepatocellular carcinoma. J Hepatol 69:182–236
8. Zech CJ, Ba-Ssalamah A, Berg T et al (2020) Consensus report from the 8th International Forum for Liver Magnetic Resonance Imaging. Eur Radiol 30:370–382
9. Hong SB, Choi SH, Kim SY et al (2021) MRI features for predicting microvascular invasion of hepatocellular carcinoma: a systematic review and meta-analysis. Liver Cancer 10:94–106
10. Wang WT, Yang L, Yang ZX et al (2018) Assessment of microvascular invasion of hepatocellular carcinoma with diffusion kurtosis imaging. Radiology 286:571–580
11. Surov A, Pech M, Omari J et al (2021) Diffusion-weighted imaging reflects tumor grading and microvascular invasion in hepatocellular carcinoma. Liver Cancer 10:10–24
12. Chong HH, Yang L, Sheng RF et al (2021) Multi-scale and multi-parametric radiomics of gadoxetate disodium-enhanced MRI predicts microvascular invasion and outcome in patients with solitary hepatocellular carcinoma ≤ 5 cm. Eur Radiol 31:4824–4838
13. Song D, Wang Y, Wang W et al (2021) Using deep learning to predict microvascular invasion in hepatocellular carcinoma based on dynamic contrast-enhanced MRI combined with clinical parameters. J Cancer Res Clin Oncol. https://doi.org/10.1007/s00432-021-03617-3
14. Lambin P, Leijenaar RTH, Deist TM et al (2017) Radiomics: the bridge between medical imaging and personalized medicine. Nat Rev Clin Oncol 14:749–762
15. Hui AM, Takayama T, Sano K et al (2020) Predictive value of gross classification of hepatocellular carcinoma on recurrence and survival after hepatectomy. J Hepatol 33:975–979
16. Rhee H, Chung T, Yoo JE et al (2020) Gross type of hepatocellular carcinoma reflects the tumor hypoxia, fibrosis, and stemness-related marker expression. Hepatol Int 14:239–248
17. Kobayashi T, Aikata H, Hatooka M et al (2015) Usefulness of combining gadolinium-ethoxybenzyl-diethylenetriamine pentaacetic acid-enhanced magnetic resonance imaging and contrast-enhanced ultrasound for diagnosing the macroscopic classification of small hepatocellular carcinoma. Eur Radiol 25:3272–3281
18. Fujinaga Y, Kadoya M, Kozaka K et al (2013) Prediction of macroscopic findings of hepatocellular carcinoma on hepatobiliary phase of gadolinium-ethoxybenzyl-diethylenetriamine pentaacetic acid-enhanced magnetic resonance imaging: Correlation with pathology. Hepatol Res 43:488–494
19. Yamazaki M, Oyanagi K, Umezu H et al (2020) Quantitative 3D shape analysis of CT images of thymoma: a comparison with histological types. AJR Am J Roentgenol 214:341–347

20. Wei SC, Xu L, Li WH et al (2020) Risk stratification in GIST: shape quantification with CT is a predictive factor. Eur Radiol 30:1856–1865

21. Jeon SK, Kim JH, Yoo J, Kim JE, Park SJ, Han JK (2021) Assessment of malignant potential in intraductal papillary mucinous neoplasms of the pancreas using MR findings and texture analysis. Eur Radiol 31:3394–3404

22. Dong SY, Yang YT, Wang WT et al (2021) Hepatobiliary phase images of gadoxetic acid-enhanced MRI may improve accuracy of predicting the size of hepatocellular carcinoma at pathology. Acta Radiol. https://doi.org/10.1177/02841851211014194

23. Choi JY, Lee JM, Sirlin CB (2014) CT and MR imaging diagnosis and staging of hepatocellular carcinoma: part I. Development, growth, and spread: key pathologic and imaging aspects. Radiology 272:635–654

24. Yang L, Gu D, Wei J et al (2019) A radiomics nomogram for preoperative prediction of microvascular invasion in hepatocellular carcinoma. Liver Cancer 8:373–386

25. Imamura H, Matsuyama Y, Tanaka E et al (2003) Risk factors contributing to early and late phase intrahepatic recurrence of hepatocellular carcinoma after hepatectomy. J Hepatol 38:200–207

26. Lee S, Kim SH, Lee JE, Sinn DH, Park CK (2017) Preoperative gadoxetic acid-enhanced MRI for predicting microvascular invasion in patients with single hepatocellular carcinoma. J Hepatol 67:526–534

27. Ariizumi S, Kitagawa K, Kotera Y et al (2011) A non-smooth tumor margin in the hepatobiliary phase of gadoxetic acid disodium (Gd-EOB-DTPA)-enhanced magnetic resonance imaging predicts microscopic portal vein invasion, intrahepatic metastasis, and early recurrence after hepatectomy in patients with hepatocellular carcinoma. J Hepatobiliary Pancreat Sci 18:575–585

28. Zhang L, Yu X, Wei W et al (2020) Prediction of HCC microvascular invasion with gadobenate-enhanced MRI: correlation with pathology. Eur Radiol 30:5327–5336

29. Ahn SJ, Kim JH, Park SJ, Kim ST, Han JK (2019) Hepatocellular carcinoma: preoperative gadoxetic acid-enhanced MR imaging can predict early recurrence after curative resection using image features and texture analysis. Abdom Radiol (NY) 44:539–548

30. Lee S, Kim KW, Jeong WK et al (2020) Gadoxetic acid-enhanced MRI as a predictor of recurrence of HCC after liver transplantation. Eur Radiol 30:987–995

31. Zhang C, Zhao R, Chen F, Zhu Y, Chen L (2021) Preoperative prediction of microvascular invasion in non-metastatic hepatocellular carcinoma based on nomogram analysis. Transl Oncol 14:100875

32. Lei Z, Li J, Wu D et al (2016) Nomogram for preoperative estimation of microvascular invasion risk in hepatitis B virus-related hepatocellular carcinoma within the Milan criteria. JAMA Surg 151:356–363